Journal of Materials Chemistry C

Accepted Manuscript

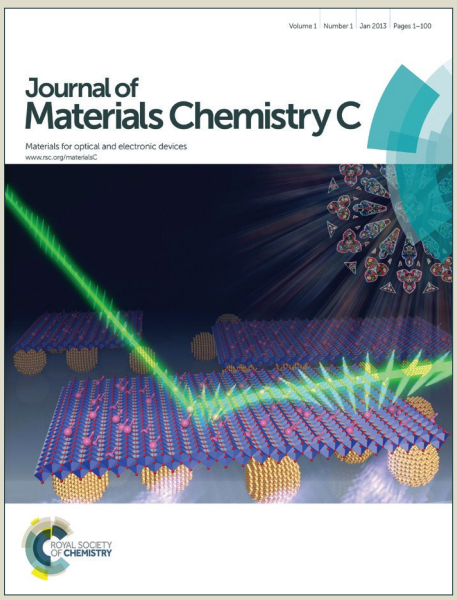

ROYAL SOCIETY OF CHEMISTRY

www.rsc.org/materialsC

Journal Name

RSCPublishing

ARTICLE

2,2'-dipyridylamino-based ligands with substituted alkyl chain groups and their mononuclear-M(II) spin crossover complexes†

Cite this: DOI: 10.1039/x0xx00000x

Received 00th January 2012,
Accepted 00th January 2012

DOI: 10.1039/x0xx00000x

www.rsc.org/

Hayley S. Scott,[a] Boujemaa Moubaraki,[a] Nicolas Paradis,[b] Guillaume Chastanet,[b] Jean-François Létard,[b] Stuart R. Batten[a,c] and Keith S. Murray,*[a]

Four new alkyl chain appended dipyridylamino-substituted-s-triazine ligands have been incorporated into seven new, mononuclear M^{II} compounds of type $[M^{II}(NCX)_2(L)_2]$ (where NCX = NCS^- or $NCSe^-$, L = *s*-triazine-dipyridylamino-based ligand and M^{II} = Fe or Co). These complexes have been structurally and magnetically characterised. The magnetic consequence of varying the alkyl chain length has been investigated in terms of intermolecular interactions and crystallographic packing arrangements. For selected complexes photomagnetic LIESST (Light-Induced Excited Spin State Trapping) measurements have been performed revealing reversible photo-induced spin-state switching.

Introduction

The coordination of alkyl-chain appended ligands to SCO[1] centres, such as Fe(II) and Co(II), has been explored in recent years in terms of the secondary functionalities that the alkyl chain groups can produce, these chains often being long and linear or branched. One of the more significant aspects of this is the formation of "soft matter" such as liquid crystals (metallomesogens)[2] and Langmuir-Blodgett films, which exhibit spin transitions. These multifunctional complexes have attracted attention from an application point of view for two reasons, liquid crystals can be easily processed into thin films still retaining their optical properties, while the incorporation of SCO centres gives the added possibility of being able to align paramagnetic liquid crystals with a magnetic field.[3] One of the first liquid crystal SCO systems, an Fe^{III} Schiff base having appended chains, was reported by Haase, Gütlich *et al*.[4] The subject has recently been extensively reviewed by Gaspar *et al*.[5] and Hayami *et al*.,[6] the former group focusing on Fe^{II} species, and the latter on Co^{II} species. Roubeau *et al.* have reported 1D Fe^{II} alkyl(C_{18})triazole liquid crystalline and Langmuir-Blodgett film SCO species.[7]

Further fundamentally interesting aspects of the use of alkyl chain-appended ligands involves investigations into structure-function relationships, for example order-disorder structural rearrangements (sometimes resulting in crystallographic phase changes), which have in the past been found to have a substantial influence on magnetic character.[8] A recent paper by Real *et al*. on an n-butylimidazole-substituted [(R-tren)Fe^{II}]$(PF_6)_2$ monomer showed an unprecedented multistable SCO material with two thermal memory channels, coupled with a phase transition, and with the scan rate dependence (temperature) of the spin transition being a feature.[9]

The work presented here is particularly pertinent to recent complexes reported by Ross *et al*.,[10] in which variable temperature single crystal structural data revealed complexes *cis*-$[Fe^{II}(DDE)_2(NCSe)_2]$ and *cis*-$[Co^{II}(DDE)_2(NCSe)_2]$ (where DDE = N^2,N^2,N^4,N^4-tetraethyl-N^6,N^6-di(pyridin-2-yl)-1,3,5-triazine-2,4,6-triamine) undergo a crystallographic phase transition (from orthorhombic *Pbcn* at high temperatures to monoclinic *P*2/*c* at low temperatures) accompanied by an order-disorder structural rearrangement of the ethyl moieties of the DDE ligand.[10]

In a general sense, long alkyl chain ligand–metal complexes can lead to formation of crystalline species, or of liquid crystals, or of mesophases. Great care and careful structural and physical measurements have to be made to identify the precise physical form of such long chain materials and of analogues having intermediate chain lengths.

The present study was focused upon the synthesis and coordination of alkyl chain- containing *s*-triazine-dipyridylamino-based ligands, and this has led to the synthesis of a mono-substituted diisopropylamino-functionalised ligand DMIP, (6-chloro-N^2,N^2-diisopropyl-N^4,N^4-di(pyridine-2-yl)-1,3,5-triazine-2,4-diamine), as well as a series of new dialkylamino-substituted ligands DPDT, (N^2,N^2,N^4,N^4-tetra-n-propyl-N^6,N^6-di(pyridin-2-yl)-1,2,5-triazine-2,4,6-triamine), DHDT, (N^2,N^2,N^4,N^4-tetra-n-hexyl-N^6,N^6-di(pyridin-2-yl)-1,2,5-triazine-2,4,6-triamine) and DODT, (N^2,N^2,N^4,N^4-tetra-n-octyl-N^6,N^6-di(pyridin-2-yl)-1,2,5-triazine-2,4,6-triamine) (Figure 1).

We report here the syntheses and properties of Fe^{II} and Co^{II} mononuclear complexes **1**-**7** (see Table 1) including structures, magnetic, photo-magnetic (LIESST; Light-Induced Excited Spin State Trapping) and heat capacity measurements on selected complexes. The study allowed us to probe metal- and ligand-dependent effects on the spin states and spin-crossover.

Table 1. Iron(II) and cobalt(II) complexes described.

		Magnetic behaviour	$\chi_M T$ (50 K)	$\chi_M T$ (300 K)	$T_{1/2}$ (K)
1	$[Fe(DMIP)_2(NCS)_2]$	Incomplete SCO	2.85↑, 2.66↓	-	70
2	$[Fe(DMIP)_2(NCSe)_2]$	Gradual SCO	0.42	3.38	160
3	$[Fe(DPDT)_2(NCS)_2]$	HS	3.54	3.64	-
4	$[Fe(DPDT)_2(NCSe)_2]$	Abrupt SCO	0.05	4.04	140
5	$[Fe(DHDT)_2(NCS)_2]$	Gradual SCO	0.84	3.59	160
6	$[Co(DHDT)_2(NCS)_2]$	HS	2.48	3.13	-
7	$[Co(DODT)_2(NCS)_2]$	HS	2.54	2.71	-

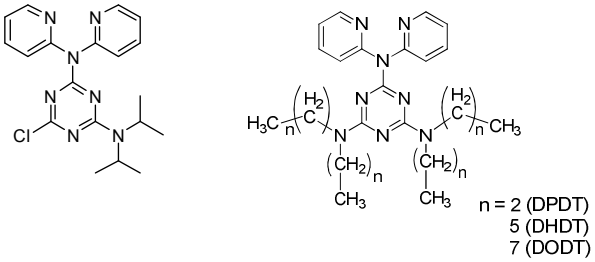

Figure 1. Molecular structure of ligands DMIP (left) and DPDT, DHDT and DODT (right).

Results and Discussion

Syntheses and characterisation

Isolation of complexes **1**-**7** was achieved either via slow vapour diffusion with diethyl ether (**1**-**2**) or slow evaporation crystallisation processes (**3**-**7**). Using these methods, crystals suitable for single crystal X-ray diffraction were collected and their structures determined, *vide infra*. Selected bond lengths, angles and distortion parameters for complexes **1**-**7** appear in Tables 2-4, while the crystallographic details appear in Table 6. In all cases, the N-donors of the dipyridylamino (dpa) group bind to the M^{II} centre, with the remaining coordination sites completed by unidentate NCX$^-$ ligands binding either *trans* (**1** and **2**) or *cis* (**3**-**7**). It was found that the longer the alkyl chain of the ligand, the more "oily" and bendy the crystals were and the harder it was to separate single crystals that were not twinned, for structural determination. Furthermore, it was found that using longer alkyl chain length ligands produced crystals coated with an oily purple substance, in the case of reactions incorporating Fe^{II} and this might be preliminary evidence for mesophase formation, at least in part.

The crystal structure of complex **4** was collected at three different temperatures (110, 140 and 185 K) in attempts to probe the existence of any order-disorder structural rearrangements influencing the spin transitions, a phenomenon which is present in a similar compound $[Fe^{II}(DDE)_2(NCSe)_2]$.[10]

In keeping with the DMIP and DPDT series (Table 1), attempts were made to synthesise the NCSe analogue of complex **5** however only a few crystals of product formed in very low yield, thus characterisation and structural data of high enough quality could not be obtained for this complex.

Octahedral distortion parameters Σ[11] and Θ[12] have been calculated for all complexes. Variable temperature structural measurements have been performed only on complex **4**, therefore $\Delta\Sigma$ and $\Delta\Theta$ values for **4** are discussed. Interestingly the microanalytical data for **1** and **2** revealed the presence of MeOH solvent molecules in bulk samples, however no solvent molecules were detected in the crystal structure. For each complex, the same sample was used for structural determination, magnetic susceptibility and IR measurements.

Structural Descriptions

Ideally, this structure section should follow the magnetic data particularly for SCO materials. However, apart from complex **4**, where temperatures for data collection were chosen from pertinent points on the susceptibility curve (see Figs 9 and 12), we have single temperature structure solutions that sometimes required use of the synchrotron (complexes **1**, **2**, **6**, **7**) for which a single temperature was fixed, thus allowing a single spin state to be probed.

Crystal structures of complexes 1 and 2

Complexes **1** and **2** are isostructural, crystallising in the monoclinic space group $P2_1/n$ with their structures determined at 100 K. These monomeric complexes consist of a central Fe^{II} which lies on an inversion centre with two DMIP ligands binding around the equatorial plane, the two remaining *trans* sites are coordinated to two NCX ligands (Figure 2). The Fe-N_{NCS} bond distances are 2.105(3) and 1.983(4) Å, while the average Fe-N_{DMIP} bond distances are 2.106 and 2.028 Å for complexes **1** and **2**, respectively. These values suggest that complex **1** exists in the HS state, while complex **2** occupies the LS state at 100 K. The *cis* N-Fe-N angles range from 87.17(11)–95.83(11)° and 87.08(16)–92.92(16)° for **1** and **2**, respectively. The crystal structure shows there are no solvent molecules present in the outer coordination spheres. There are intramolecular H-bonds between N7…(C18)H18 (2.207 Å for **1** and 2.202 Å for **2**) of the same ligand. There is also an NCX…$centroid_{triazine}$ interaction within the same complex for **1** and **2** with distances of 3.620 Å and 3.656 Å, respectively. Selected bond lengths and angles for complexes **1**-**7** appear in

Tables 2-3. The packing diagram along the *c*-axis for **1** and **2** appears in Figure S1.

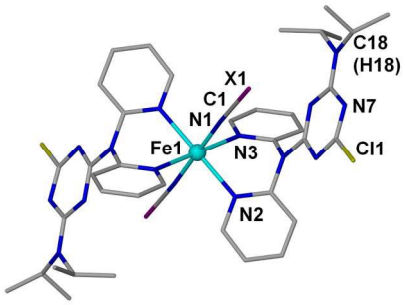

Figure. 2. Structure of the mononuclear complex **1** (isostructural to **2**). X = S, Se.

Crystal structures of complexes 3 and 4

Complexes **3** and **4** are isostructural and crystallise in the orthorhombic space group *Pbcn*. Similar to the DMIP series, two DPDT ligands are coordinated to the Fe^{II} centre, binding via the dpa N-donors. However, unlike the DMIP series, these ligands bind in a *cis*-arrangement, leaving two *cis*-sites that are coordinated to two NCX ligands (Figure 3).

For complex **3**, at 123 K, the Fe-N_{NCS} bond lengths are 2.114(11) Å, while the average Fe-N_{DPDT} bond distances are equal to 2.204 Å. These values are suggestive of the complex occupying the HS state at this temperature. The *cis* and *trans* angles range between 81.66(4)-95.09(4)° and 168.28(5)-173.76(4)°, respectively. No solvent molecules were present in the outer coordination sphere. π-π stacking occurs between adjacent complexes, with C10…$centroid_{pyridyl}$ distances equal to 3.451 Å in **1** (Figure 4).

Due to the abrupt spin transition behaviour of complex **4** (see below), the crystal structure of **4** was collected at three different temperatures, 110, 140 and 185 K in attempts to analyse the presence of any order-disorder structural rearrangements associated with the crossover, a phenomenon which has already been observed in similar complexes.[10]

For complex **4**, the Fe-N_{NCSe} bond distances are equal to 1.957(3), 2.094(2) and 2.127(2) Å, while the average Fe-N_{DPDT} bond distances are equal to 1.989, 2.184 and 2.195 Å, for measurements made at 110, 140 and 185 K, respectively. The *cis* N-Fe-N angles range between 86.03(8)–96.99(7)°, 83.11(8)–96.14(11)° and 82.04(8)–95.94(11)°, while *trans* angles range between 174.49(8)–177.26(7)°, 172.07(11)–173.94(9)° and 170.85(11)–173.51(9)° at temperatures 110, 140 and 185 K, respectively. The octahedral distortion parameter, Σ[10], was found to equal 29°, 40° and 44°; while Θ[11] was calculated to be 70º, 107º and 117º at 110, 140 and 185 K, respectively. In accordance with previous studies, distortion parameters Σ and Θ become higher as the diffraction temperature is increased (*i.e.* moving towards transition to the HS state), as the distortion of the first coordination sphere octahedron is increased going to the HS form. No solvent molecules were found to exist in the outer coordination sphere. The π-π stacking observed in **3** is also present in **4** with C10…centroid separations increasing with higher temperature collections. C10…centroid distances of 3.479, 3.487 and 3.511 Å were observed at 110, 140 and 185 K, respectively.

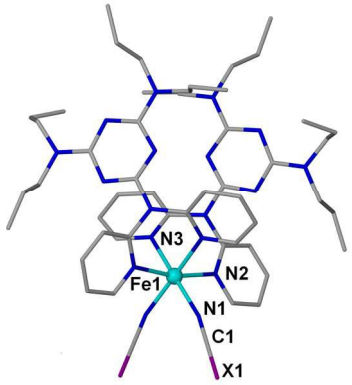

Fig. 3. Structure of complex **3** (isostructural to **4**). X = S, Se.

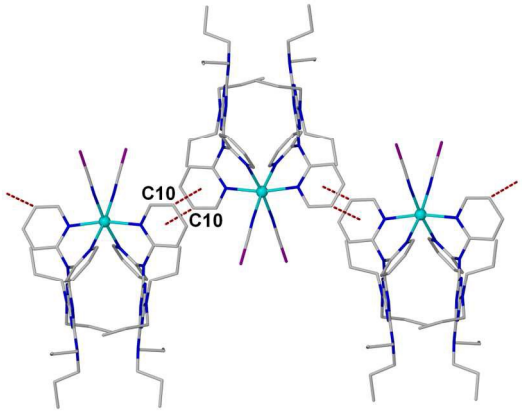

Fig. 4. Packing along *a*-axis of complex **3** (isostructural to **4**).

Crystal structure of complex 5

Complex **5** crystallises in the monoclinic space group *C*2/*c* and its structure was collected at 123 K. Eight monomers exist per unit cell with the asymmetric unit making up two discrete half monomers, (*i.e.* two structurally distinct monomers with centres of inversion). The binding modes of the ligands for both monomers are the same and are consistent with those of the DPDT series with two dpa groups from two ligands binding in the *cis* arrangement and two NCS$^-$ ligands completing the coordination sphere (Figure 5). The Fe-N_{NCS} bond distances are 2.055(6) and 2.118(6) Å, while the average Fe-N_{DHDT} bonds are equal to 2.125 and 2.199 Å for Fe1 and Fe2, respectively. *Cis* N-Fe-N angles range between 83.63(19)-93.96(19)° and 82.78(19)–96.10(3)º; while *trans* angles range between 176.5(2)-176.76(3)° and 174.80(2)–177.80(3)º for Fe1 and Fe2, respectively. The S-S distances between *cis*-NCS groups differs considerably between the two monomers. For the Fe1 complex, the two NCS groups appear to be almost parallel with one another, with the S-S distances equal to 5.266 Å. However, the NCS groups on the Fe2 complex are extended and direct away from one another, the S-S distance is 8.589 Å. No solvent molecules were present in the outer coordination sphere. There are close CH...π contacts between pyridyl rings of adjacent monomers {C41(H41)...C9 3.107 Å, C42(H42)...C11 3.085 Å} (Figure 6). The closest Fe...Fe distance (between Fe1 and Fe2) is 9.1360(18) Å, while closest Fe1...Fe1 and Fe2...Fe2 distances are equal to 15.377(3) and 16.682(5) Å, respectively. One of the C6 alkyl chain arms is disordered, in the Fe2 monomer (C55 to C58), and the disorder has been modeled (see X-ray Crystallography in Experimental for further details). A packing diagram of **5** along the c-axis appears in Figure S2.

Crystal structure of the Co^{II} complexes 6 and 7

Compound **6** crystallises in the orthorhombic space group $P2_12_12_1$ and its structure was collected at 100 K. While not isomorphous to complex **5** the binding modes of the ligands are the same (Figure S3). The Co-N_{NCS} and Co-N_{DHDT} bond lengths have an average distance of 2.079 Å and 2.153 Å, respectively. These bond lengths indicate that the Co^{II} occupies the HS state at this temperature. The *cis* and *trans* angles range between 81.72(8)–97.28(9)° and 172.07(9)-177.01(8)°, respectively. There are no intermolecular interactions or solvent molecules in the outer coordination sphere.

Complex **7** crystallises in the triclinic space group *P*-1 and its structure was collected at 173 K. The asymmetric unit consists of two full monomeric units. The binding modes of the ligands are the same as those for the analogous compounds **5** and **6** and the structure is shown in Figure 7. The Co-N_{NCS} bond lengths have an average distance of 2.067 and 2.046 Å, for Co1 and Co2 centres, respectively; average Co-N_{DODT} bond lengths are equal to 2.160 and 2.169 Å for Co1 and Co2 centres, respectively. These bond lengths indicate the Co^{II} occupies the HS state at this temperature. The N-Co-N *cis* angles range between 82.0(2)–98.2(2)° and 81.0(2)–101.5(2)° for Co1 and Co2, respectively. *Trans* angles range between 171.4(2)–179.0(3)° and 166.4(2)–175.8(3)° for Co1 and Co2, respectively. There are no solvent molecules present in the outer coordination sphere. There are also no strong intermolecular interactions between complexes. Complex **7** packs in such a way that there are distinct regions rich in Co^{II} centres or alkyl chain regions (Figure S4).

Journal Name RSCPublishing

ARTICLE

Table 2. **Summary of selected bond lengths and octahedral distortion parameters for compounds 1-7**.

	1	**2**	**3**	**4** (110K)	**4** (140 K)	**4** (185 K)	**5**(Fe1)	**5**(Fe2)	**6**	**7**(Co1)	**7**(Co2)
T/K	100	100	123	110	140	185	123	123	100	173	173
M-N_{NCX} (Å) (av.)	2.105(3)	1.983(4)	2.1139(11)	1.957(3)	2.094 (2)	2.127 (2)	2.104(7)	2.105(6)	2.0795	2.067	2.046
M-N_{py} (Å) (av.)	2.106	2.028	2.204	1.989	2.149	2.195	2.214	2.403	2.153	2.160	2.169
M-N-C_{NCX} (°)	172.1(3)	171.8(4)	165.90(11)	168.0(3)	167.1(2)	166.9(2)	152.5(6)	149.0(5)	178.6(3)	168.1(7), 158.1(7)	158.5(5), 161.0(6)
Σ^a	35	36	43	29	40	44	25	39	43	45	59
Θ^b	53	34	124	70	107	117	57	78	97	116	165
M…M_{inter} [c]	10.787(2)	10.763(2)	8.9023(3)	8.8676(11)	8.9947(7)	9.0464(7)	15.377(3)	16.682(5)	8.9280(18)	8.815(4)	8.659(5)

[a] derived from the N-Fe-N angles and is the sum of the deviations from 90° of the 12 *cis* N-Fe-N angles in the coordination sphere, Σ is equal to 0 for an ideal octahedron and increases with the deformation; ref 11. [b] The parameter Θ describes the deviation in coordination geometry from perfectly octahedral (O_h) to a trigonal prismatic structure (D_{3h}) for a $M^{II}N_6$ centre1; ref. 12. [c] The closest M…M contact.

Table 3. **Selected bond lengths and angles for complexes 1-4**.

Bond(s)	1	2	3	4 (110K)	4 (140K)	4 (185K)
Lengths (Å)						
N(1)-Fe(1)	2.105(3)	1.983(4)	2.1139(11)	1.957(3)	2.094(2)	2.127(2)
N(2)-Fe(1)	2.205(3)	2.025(4)	2.1828(10)	1.985(3)	2.133(2)	2.178(2)
N(3)-Fe(1)	2.208(3)	2.032(4)	2.2266(10)	1.993(3)	2.163(2)	2.212(2)
N(1')-Fe(1)	2.105(3)	1.983(4)	2.1142(11)	1.957(3)	2.094(2)	2.127(2)
N(2')-Fe(1)	2.205(3)	2.025(4)	2.1828(10)	1.985(3)	2.133(2)	2.178(2)
N(3')-Fe(1)	2.208(3)	2.032(4)	2.2266(10)	1.993(3)	2.163(2)	2.212(2)
Angles (°)						
N(1)-Fe-N(2)	90.75(12)	88.60(17)	88.68(4)	89.74(12)	92.77(13)	93.34(9)
N(1)-Fe-N(3)	92.18(12)	87.33(16)	95.08(4)	88.43(12)	88.58(8)	88.65(8)
N(1')-Fe-N(1)	180.0(2)	180.00(3)	88.06(6)	86.18(17)	86.98(13)	87.13(13)
N(1)-Fe-N(2')	89.25(12)	91.40(16)	173.76(4)	92.25(12)	92.98(9)	93.29(9)
N(1)-Fe-N(3')	87.82(12)	92.67(16)	93.33(4)	174.48(12)	173.94(9)	173.52(9)
N(2)-Fe-N(3)	84.17(11)	87.08(16)	81.66(4)	86.54(12)	83.11(8)	82.05(8)
N(1')-Fe-N(2)	89.25(12)	91.40(16)	173.76(4)	92.25(12)	92.98(9)	93.29(9)
N(2)-Fe-N(2')	180.0(2)	180.00(1)	95.06(5)	177.28(16)	172.07(11)	170.84(11)
N(3')-Fe-N(2)	95.83(11)	92.92(16)	90.42(4)	91.66(12)	91.57(8)	91.80(8)
N(1')-Fe-N(3)	87.82(12)	92.67(16)	93.33(4)	174.48(12)	173.94(9)	173.52(9)
N(2')-Fe-N(3)	95.83(11)	92.92(16)	90.42(4)	91.66(12)	91.57(8)	91.8(8)
N(3')-Fe-N(3)	180.0(3)	180.00(1)	168.29(5)	96.98(16)	96.14(11)	95.96(11)
N(1')-Fe-N(2')	90.75(12)	88.60(17)	88.68(4)	89.74(12)	92.77(13)	93.34(9)
N(1')-Fe-N(3')	92.18(12)	87.33(16)	9.08(4)	88.43(12)	88.58(8)	88.65(8)
N(3')-Fe-N(2')	84.17(11)	87.08(16)	81.66(4)	86.54(12)	83.11(8)	82.05(8)

Table 4. **Selected bond lengths and angles for complexes 5-8**.

Bond(s)	**5** (Fe1)	**Bond(s)**	**5** (Fe2)	**Bond(s)**	**6**	**7** (Co1)	**Bond(s)**	**7** (Co2)
Lengths (Å)		***Lengths (Å)***		***Lengths (Å)***			***Lengths (Å)***	
N(1)-Fe(1)	2.041(7)	**N(10)-Fe(1)**	2.105(6)	**N(1)-Co(1)**	2.074(2)	2.058(7)	**N(19)-Co(2)**	2.044(7)
N(2)-Fe(1)	2.104(6)	**N(11)-Fe(1)**	2.190(5)	**N(2)-Co(1)**	2.085(2)	2.076(8)	**N(20)-Co(2)**	2.047(6)
N(3)-Fe(1)	2.110(5)	**N(12)-Fe(1)**	2.213(5)	**N(3)-Co(1)**	2.123(2)	2.155(6)	**N(21)-Co(2)**	2.161(5)
N(1')-Fe(1)	2.041(7)	**N(10')-Fe(1)**	2.105(6)	**N(4)-Co(1)**	2.174(2)	2.163(6)	**N(22)-Co(2)**	2.152(7)
N(2')-Fe(1)	2.104(6)	**N(11')-Fe(1)**	2.190(5)	**N(5)-Co(1)**	2.161(2)	2.179(7)	**N(23)-Co(2)**	2.205(6)
N(3')-Fe(1)	2.110(5)	**N(12')-Fe(1)**	2.213(5)	**N(6)-Co(1)**	2.157(2)	2.144(5)	**N(24)-Co(2)**	2.157(6)
Angles (°)		***Angles (°)***		***Angles (°)***			***Angles (°)***	
N(1)-Fe-N(2)	89.7(2)	**N(10)-Fe-N(11)**	93.3(2)	**N(1)-Co-N(2)**	97.28(9)	96.0(3)	**N(19)-Co-N(20)**	97.8(3)
N(1)-Fe-N(3)	89.9(2)	**N(10)-Fe-N(12)**	174.8(2)	**N(1)-Co-N(3)**	92.26(9)	90.7(2)	**N(19)-Co-N(21)**	87.1(2)
N(1')-Fe-N(1)	90.0(3)	**N(10')-Fe-N(10)**	96.0(3)	**N(1)-Co-N(4)**	172.17(9)	171.6(2)	**N(19)-Co-N(22)**	166.4(2)
N(1)-Fe-N(2')	93.0(2)	**N(10)-Fe-N(11')**	88.4(2)	**N(1)-Co-N(5)**	87.93(9)	88.5(3)	**N(19)-Co-N(23)**	87.8(2)
N(1)-Fe-N(3')	177.0(2)	**N(10)-Fe-N(12')**	87.5(2)	**N(1)-Co-N(6)**	90.72(9)	89.2(2)	**N(19)-Co-N(24)**	89.6(2)
N(2)-Fe-N(3)	84.0(2)	**N(11)-Fe-N(12)**	83.1(2)	**N(2)-Co-N(3)**	89.68(9)	89.0(2)	**N(20)-Co-N(21)**	87.9(2)
N(1')-Fe-N(2)	93.0(2)	**N(10')-Fe-N(11)**	88.4(2)	**N(2)-Co-N(4)**	87.74(9)	88.2(2)	**N(20)-Co-N(22)**	90.7(2)
N(2)-Fe-N(2')	176.2(3)	**N(11)-Fe-N(11')**	177.5(3)	**N(2)-Co-N(5)**	172.07(9)	171.4(2)	**N(20)-Co-N(23)**	169.3(2)
N(3')-Fe-N(2)	93.3(2)	**N(12')-Fe-N(11)**	95.1(2)	**N(2)-Co-N(6)**	90.10(9)	90.0(2)	**N(20)-Co-N(24)**	89.9(2)
N(1')-Fe-N(3)	177.0(2)	**N(10')-Fe-N(12)**	87.5(2)	**N(3)-Co-N(4)**	81.72.(8)	82.0(2)	**N(21)-Co-N(22)**	82.6(2)
N(2')-Fe-N(3)	93.3(2)	**N(11')-Fe-N(12)**	95.1(2)	**N(3)-Co-N(5)**	96.10(8)	98.2(2)	**N(21)-Co-N(23)**	101.5(2)
N(3')-Fe-N(3)	90.3(3)	**N(12')-Fe-N(12)**	89.1(3)	**N(3)-Co-N(6)**	177.01(8)	179.0(3)	**N(21)-Co-N(24)**	175.8(3)
N(1')-Fe-N(2')	89.7(2)	**N(10')-Fe-N(11')**	93.3(2)	**N(4)-Co-N(5)**	87.73(8)	88.2(2)	**N(22)-Co-N(23)**	85.6(2)
N(1')-Fe-N(3')	89.9(2)	**N(10')-Fe-N(12')**	174.8(2)	**N(4)-Co-N(6)**	95.29(8)	98.1(2)	**N(22)-Co-N(24)**	101.1(2)
N(3')-Fe-N(2')	84.0(2)	**N(12')-Fe-N(12')**	89.1(3)	**N(5)-Co-N(6)**	83.84(8)	82.8(2)	**N(23)-Co-N(24)**	81.0(2)

Journal Name

RSCPublishing

ARTICLE

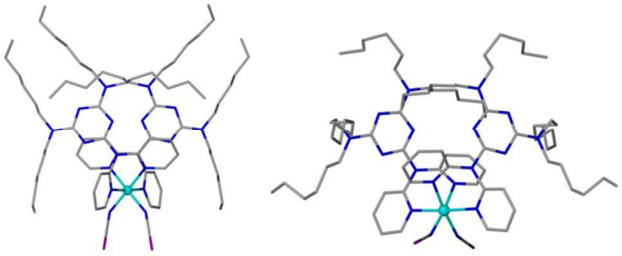

Figure 5. Molecular structure of **5**. (Left) Fe1 monomer, (Right) Fe2 monomer. H atoms omitted for clarity

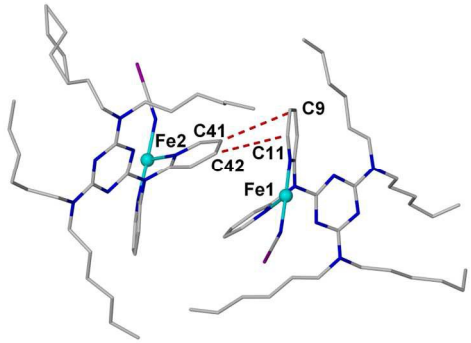

Figure 6. Closest point contacts for complex **5**.

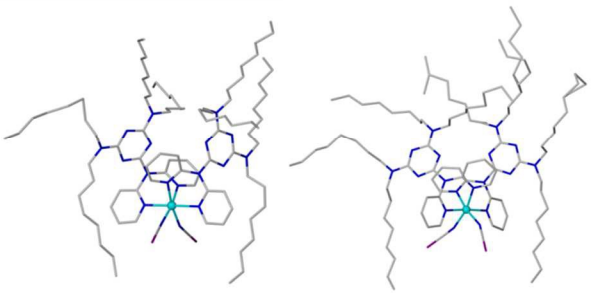

Figure 7. Structure of complex **7**. (Left) Co1 monomer, (Right) Co2 monomer. Some of the alkyl chains in Co2 monomer are disordered.

Magnetic behaviour of polycrystalline samples

The thermal dependence of $\chi_M T$ for complexes **1** and **2**, over the temperature range of 5–250 K, is shown in Figure 8. Compound **1** was found to undergo a gradual and (very) incomplete spin transition. At 250 K a $\chi_M T$ value of 3.5 cm^3 mol^{-1} K is observed and this HS value gradually decreases to 100 K, at which point a more rapid decrease is observed upon cooling to 60 K, giving a $\chi_M T$ value of 2.6 cm^3 mol^{-1} K. Here a plateau in $\chi_M T$ is seen with further decreases in $\chi_M T$ below ~10 K attributed to zero field splitting, with a final $\chi_M T$ of 2.3 cm^3 mol^{-1} K reached at 5 K. The discontinuity of $\chi_M T$ observed below 60 K, upon cooling and heating, is due to HS thermal trapping under rapid cooling, as seen by the higher $\chi_M T$ values found on warming between 5 and 60 K. The incomplete spin-transition is confirmed in the LIESST study, *vide infra*; Fig. S5 in ESI. We have reported other Fe^{II} SCO species that show kinetic trapping at low temperatures.[13]

Compound **2** undergoes a gradual spin transition, with $T_{1/2}$ occurring close to 160 K. At 250 K a $\chi_M T$ value of 3.30 cm^3 mol^{-1} K was measured, typical of HS Fe^{II}, a little less than in **1**, this value gradually decreasing on cooling to 190 K, at which point a more rapid decrease is observed to 100 K giving a $\chi_M T$ value of 0.4 cm^3 mol^{-1} K at this temperature, indicative of LS Fe^{II}, confirmed by the crystallographic Fe-N values. Further cooling to 10 K yields a plateau with a final $\chi_M T$ of 0.3 cm^3 mol^{-1} K. The spin transition has a hint of thermal hysteresis.

Complex **3** remains HS over the temperature range 2-300 K with a $\chi_M T$ value of 3.7 cm^3 mol^{-1} K remaining essentially constant, as shown in Figure 9. The rapid decrease in $\chi_M T$ at lower temperatures is due to zero field splitting. The data are compatible with the crystallographic study at 123 K.

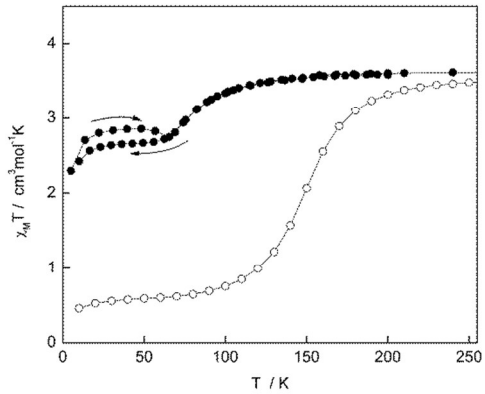

Figure 8. $\chi_M T$ vs. T data for compounds **1**(▪) and **2**(▫). Heating and cooling cycles for **2** have essentially the same values. Applied dc field = 1T.

Complex **4**, which contains the stronger ligand field NCSe ligands, reveals an abrupt spin-transition with $T_{1/2}$ occurring at 140 K (Figure 9). At room temperature, a starting $\chi_M T$ value of 4.0 cm^3 mol^{-1} K remains essentially constant following cooling to 150 K at which point a very abrupt spin transition occurs and a $\chi_M T$ value of 0.1 cm^3 mol^{-1} K is observed at 110 K. This value remains constant following further cooling to 2 K. To further investigate possible thermal hysteresis in complex **4**, differential scanning calorimetry (DSC) was used to measure the heat flow between 145 K and 130 K. A well developed endothermic peak situated at 139 K, characteristic of a first-order phase transition, was observed (Figure 10). An exothermic peak was observed at 135 K, during the cooling cycle, shifted by ~3 K from the endothermic peak and thus potentially indicates the occurrence of a very small thermal hysteresis ΔT. From these data the entropy and enthalpy of the transition between the LS and HS states were determined to be ΔH = 4.468 kJ mol^{-1} and ΔS = 32.478 J mol^{-1} K^{-1}. The thermal behaviour was consistent throughout repeat heating and cooling cycles. Furthermore, the DSC data are in good agreement with the magnetic data shown in Figure 9. The values of enthalpy and entropy changes are normal for such Fe^{II} centres and suggest the coupling of the electronic and phonon states are operative as discussed by Sorai and Seki.[14]

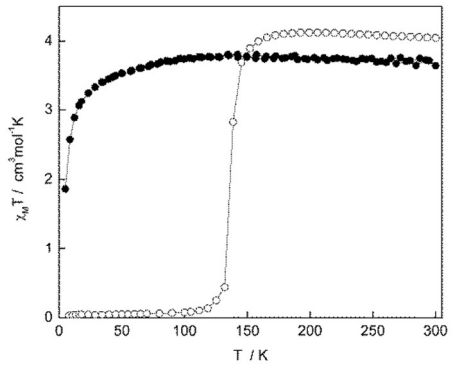

Figure 9. $\chi_M T$ vs. T data for compounds **3**(●) and **4**(○). Applied dc field = 1 T. Scan rate = 10 K/min.

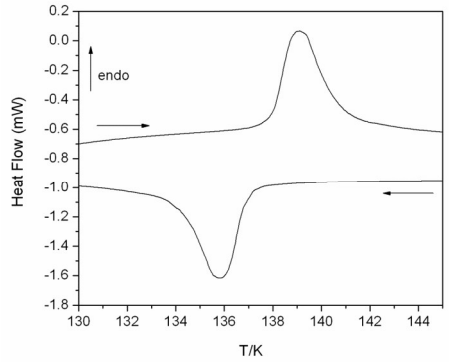

Figure 10. The differential scanning calorimetric measurement for a single heating and cooling cycle of **4** between 145 K and 130 K. The arrows indicate the direction of the cycle and the endothermic peaks point upward as indicated. Scan rate = 5 K/min.

The thermal dependence of $\chi_M T$ for complex **5** is shown in Figure 11. Compound **5** was found to undergo a gradual and somewhat unusually shaped spin transition, with $T_{1/2}$ occurring close to 160 K. At room temperature a $\chi_M T$ value of 3.7 cm^3 mol^{-1} K remains constant following cooling to 220 K after which point the $\chi_M T$ continually decreases gradually, with temperature, to show a LS plateau below ~50 K, reaching a value of 0.4 cm^3 mol^{-1} K at 2 K. Thermal hysteretic behaviour was not observed in the heating and cooling modes. At 123 K the Fe-N bond lengths, determined from the crystal structure, suggest the complex should occupy the HS state, however the magnetic data indicates occupation of the LS state for **5** at this temperature. The most likely reason for this discrepancy could be due to HS trapping as the crystal is quenched cooled under the cryostream for structural analysis.

Compound **6** was found not to show any d^7 S = 3/2 to S = 1/2 SCO properties over the temperature range 2–300 K (Figure 11). A $\chi_M T$ value of 3.1 cm^3 mol^{-1} K (μ_{eff} = 4.98 μ_B) at room temperature, typical of octahedral Co^{II} complexes, remains constant with cooling down to 100 K, after which point a slow decrease in $\chi_M T$ value occurs, where a more rapid decrease below 5 K to reach a final value of 1.6 cm^3 mol^{-1} K (μ_{eff} = 3.58 μ_B) at 2 K. Similarly, complex **7** also remains HS between 5-300 K. A slightly lower $\chi_M T$ value of 2.7 cm^3 mol^{-1} K was measured at 300 K and this value remains essentially constant, with a gentle increase, upon cooling to 50 K, at which point a gradual decrease in $\chi_M T$ to 1.9 cm^3 mol^{-1} K was measured at 5 K. This behaviour is typical of HS octahedral d^7 ions that have $^4T_{1g}$ ground states in pure octahedral symmetry, yielding temperature dependent $\chi_M T$ values, the precise shapes depending on distortions from O_h symmetry and spin-orbit coupling.[15] The same situation occurred in the case of the siblings $[Fe^{II}(DDE)_2(NCSe)_2]$ and $[Co^{II}(DDE)_2(NCSe)_2]$, where the Fe^{II} species showed spin-crossover ($T_{1/2}$ ~270 K) and the Co^{II} complex remained HS at all temperatures.[10]

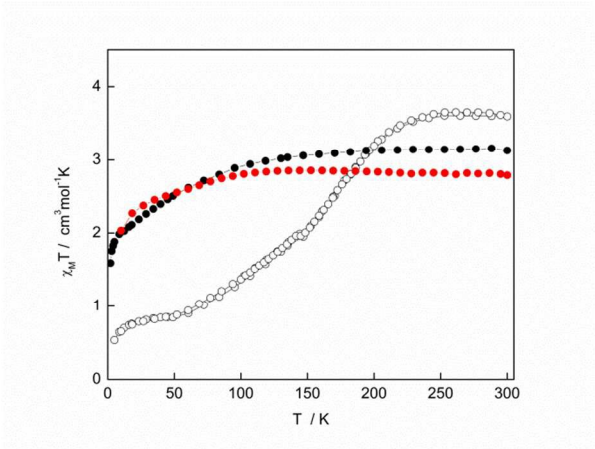

Figure 11. $\chi_M T$ vs. T data for compounds **5**(○), **6**(●), and **7**(● red). Applied dc field = 1 T. Scan rate = 10 K/min.

LIESST studies on complexes 1, 2 and 4

Photomagnetic LIESST studies were carried out on compounds **1**, **2** and **4**. The LIESST results for **1**, **2** and **4** were similar and so only the Figures for the LIESST and kinetics measurements of 4 are shown here (Figures for **1** and **2** are located in the ESI).

The thermal spin-transition curves of the samples (thin layers) have been recorded to calibrate the photomagnetic data to the bulk measurements obtained previously. Light irradiation was tested at different wavelengths and the best one was found to be in the green region (510 nm) with a 5 mW/cm^2 power laser. For **1** and **2**, only the LIESST effect was observed and not reverse-LIESST, however both LIESST and reverse-LIESST were observed for complex **4**. When the photostationary limit was reached, the T(LIESST) curve was recorded (Figures 12 and S5-S6). The increase of $\chi_M T$ from 10 to 30 K observed for **1** and **2** usually follows from the Fe^{II} HS zero-field splitting (zfs). The maximum $\chi_M T$ value gives some information on the photoconversion efficiency that is around 92 % for **1**, 100 % for **2** and 75% for **4**. Above 40 K the $\chi_M T$ product decreases and the baseline is recovered. The minimum value of the derivative $\delta\chi_M T/\delta T$ gives the value of the T(LIESST) temperature estimated at 60 K for **1**, 48 K for **2** and 55 K for **4** (Table 5). It should be noted that the low value of $T_{1/2}$ for **1** (around 75 K) with a close T(LIESST) value (around 60 K) could induce an inhibition of the thermal SCO and induces a huge HS residue at low temperature.[16]

Table 5. LIESST data obtained for complexes 1, 2 and 4; [a]Obtained from bulk measurement; [b]Obtained from the photomagnetic measurement. [c]σ is the Gaussian distribution. [d]This value is E_a^*.

	$T_{1/2}$[a] (K)	$T_{1/2}$[b] (K)	T(LIESST)	E_a (cm^{-1})	k_∞ (s^{-1})	σ (cm^{-1})[c]
1	79/80	76	60	830	4.5 10^5	52
2	146	145	48	360	6.0 10^1	36
4	140	140	55	610	1.5 10^3	160[d]

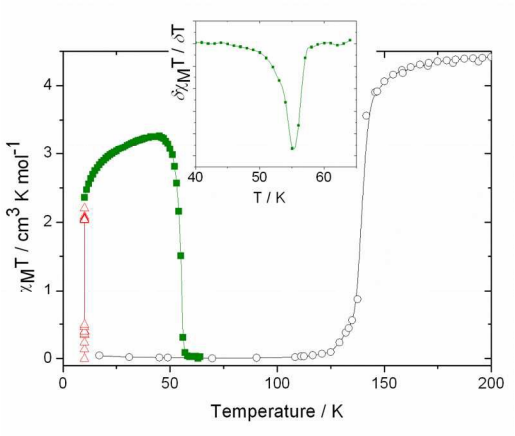

Figure 12. Thermal behaviour of the $\chi_M T$ product of **4** before irradiation showing reproducibility on cycling (o), during irradiation (Δ) and in the dark after irradiation (●). The insert presents the derivative of the thermal behaviour in the dark after irradiation, the minimum of which allows the determination of the T(LIESST) value. See Experimental for scan rate details.

For complex **4**, if irradiation at 830 nm is applied, a decrease of the HS fraction is observed. After one hour, half of the molecules are converted back to the LS state (Figure 13). This decrease could follow from either natural relaxation of the HS state or the reverse-LIESST effect. To discriminate between the two effects, a relaxation in the dark was recorded after a new irradiation at 510 nm to saturate the HS population. Figure 13 shows that the HS fraction remains constant in the dark at 10 K, therefore, the decrease observed under irradiation at 830 nm is due to the reverse-LIESST effect.

Since **3** and **4** are isostructural and very similar in terms of coordination sphere, reverse-LIESST was tested on **3**. However, no effect was observed and the compound remains HS.

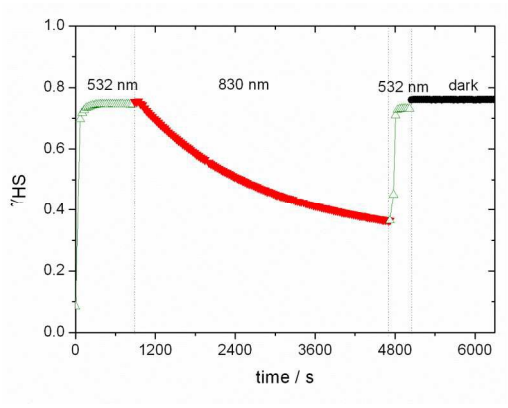

Figure 13. Evolution of the HS fraction of **4** at 10 K under 532 nm irradiation (Δ), 830 nm (▼) and in the dark (●) after photo-excitation at 532 nm.

Several kinetics experiments have also been performed on complexes **1**, **2** and **4** in order to characterise the relaxation process after irradiation (Figures 14 and S7-S8). For **1** and **2**, the relaxation curves follow an exponential shape. A particular point should be noted on compound **1** for which the kinetics slightly relax below the baseline confirming the kinetic trapping of the spin-crossover. To extract the relaxation rate constant at each temperature, a stretched exponential law was applied, with a Gaussian distribution σ of the activation energy.[17] The fit of the kinetics is shown in Figure 14 for **2**. The thermodynamic parameters E_a, k_∞ and σ were extracted from the Arrhenius plot (ln k_{HL} *vs* 1/T) and are summarised for **1**, **2** and **4** in Table 5 with the relaxation constant

$$k_{HL}(T) = k_\infty.\exp(-E_a/k_BT) \qquad \text{eq. 1}$$

where the pre-exponential factor k_∞ is k_{HL} at T → ∞, and E_a the activation energy.

For compound **4**, the relaxation curves follow a sigmoidal behaviour in agreement with the cooperative character of the thermal spin transition. To extract the relaxation rate constant at each temperature, we have considered the self-accelerated model[18] in which the relaxation rate $k_{HL}(T,\gamma_{HS})$ depends on the HS fraction along the relaxation according to equation 2. In this equation $k_{HL}(T)$ comes from equation 1 and E_a* is the additional activation energy due to the cooperative character of

the material. Figure 14 reports the fit of the kinetics obtained with this approach. The thermodynamic parameters Ea, k∞ and Ea* were extracted from the Arrhenius plot (ln k_{HL} vs 1/T, insert Figure 14) and are summarized in Table 5.

$$k_{HL}(T,\gamma_{HS}) = k_{HL}(T).\exp[(1-\gamma_{HS}).E_a^*/k_BT] \quad \text{eq. 2}$$

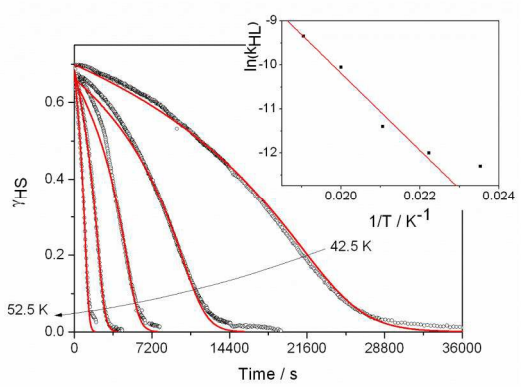

Figure 14. Plot of the different relaxation kinetics recorded as function of the temperature for **4**. The red lines are the fits discussed in the text.

Unfortunately we do not have LIESST or relaxation kinetics on complex **5**, for which the unusual $\chi_M T$ vs. T plot is shown in Fig. 11. We anticipate photomagnetism of the kind reported for a similar gradual LS-HS transition seen in a 1D Fe^{II} compound.[19]

Discussion

In the structural context, complexes **3** and **4** are very similar to the previous DDE complexes studied by Ross *et al*.,[10] which showed temperature dependent order-disorder phase transitions. The occurrence of the concomitant order-disorder and crystallographic phase transitions in *cis*-$[Fe^{II}(DDE)_2(NCSe)_2]$ and *cis*-$[Co^{II}(DDE)_2(NCSe)_2]$ were not directly apparent in their magnetic susceptibility measurements, and this was likely due to the local environment of the M^{II} centres remaining largely undisturbed as the transitions occur. Surprisingly, using a series of very similar ligands to DDE, here, and incorporating these into a family of analogous complexes of type *cis*-$[Fe^{II}(L)_2(NCX)_2]$, we did not observe any crystallographic phase transitions, perhaps more surprisingly in the case of complex **4**, which shows a very abrupt spin-transition.

Both **3** and **4** display π-π stacking between complexes. The highly cooperative nature of the spin transition for complex **4** (which shows an abrupt SCO with small hysteresis) is likely due to a combination of intermolecular π-π effects and the stronger ligand field strength afforded by the $NCSe^-$ ligand, compared with NCS for **3**.

Because structural data on complex **5** have only been collected at one temperature (123 K) we cannot confirm the absence of a change in phase in the Fe2 complex that displayed disorder, however, looking at the very gradual nature of the spin transition (Figure 11), it seems unlikely that any possible structural phase change would influence the magnetic behaviour of the complex.

In the case of the two HS Co^{II} complexes **6** and **7**, there is no SCO and thus no evidence for "reverse" SCO of the kind proposed in Hayami's $[(R\text{-terpy})_2Co]^{2+}$ salts where R is a long chain e.g. C_{16}.[20] The present $[Co(L)_2(NCX)_2]$ compounds, of course have different stoichiometries and are neutrally charged, with L = DODT having only a C_8 chain.

Ligand field considerations

The magnetic properties of the present complexes show that SCO occurs in the Fe^{II} complexes **1**, **2**, **4** and **5**, while **3** and the Co^{II} complexes **6** and **7** remain HS at all temperatures. The $NCSe^-$ derivatives, **2** and **4**, with their stronger ligand-fields, compared to NCS^- (in **1** and **3**) both show SCO. For a constant NCS^-/Fe^{II} coordination, it can be seen that the order of decreasing ligand field, when assuming that crystal packing effects, *etc*. are minimal, are DHDT>DMIP>DPDT. The two $NCSe^-$ complexes follow the same trend. In view of the abrupt spin transition in complex **4**, this would suggest that cooperativity is strongest in this case.

Photomagnetic measurements

Regarding the photomagnetic studies, compounds **1**, **2** and **4** are sensitive to the LIESST effect and T(LIESST) values were measured giving values of 60 K for **1**, 48 K for **2** and 55 K for **4**, which all belong to the T_0 = 100 K line in the graph of T(LIESST) *vs*. $T_{1/2}$,[20] where $T(\text{LIESST}) = T_0 - 0.3T_{1/2}$. From a database on many mononuclear FeN_6 coordination environments, this line is indicative of $FeN_4(NCX)_2$ coordination spheres, as expected.[21] Moreover, with stronger NCX ligand fields we would expect higher $T_{1/2}$ and lower T(LIESST) values. Compounds **1**, **2** and **4** clearly follow this trend.

Octahedral distortion

Parameters Σ and Θ have been calculated in this work to quantify the octahedral distortion around the M^{II} centre. For complex **4**, ΔΣ was calculated to equal 15°, while ΔΘ was equal to 40°, thus signifying an increase in the octahedral distortion as the spin transition occurs from LS to HS.

For complex **5**, Σ and Θ for Fe1 and Fe2 differ significantly. Σ is equal to 25° and 39° for Fe1 and Fe2, respectively, while Θ is equal to 57° and 78° for Fe1 and Fe2, respectively. These values suggest that Fe2 is in a much more distorted geometry than Fe1, and it also may suggest that the SCO behaviour of each of these is unique (*ie*. the "crossover point" for each of these occurs at different temperatures).

Similar to the situation in **5**, there are significant differences in octahedral distortion parameters between the Co1 and Co2 centres in complex **7**. Both Σ and Θ suggest the Co2 site occupies a much more distorted octahedral geometry than does the Co1 site.

Comments on synthesis

Attempts to form Fe/DODT complexes, analogous to **7**, were made however recovery of a solid crystalline product was not achieved. It was generally found that, as the alkyl chain length was increased, it became more difficult to form the Fe^{II} derivatives of the appropriate complexes. No such problems were observed in the synthesis of the Co^{II} complexes.
Synthesis of a di-substituted diisopropyl-based ligand (analogous to DMIP) was attempted, however despite numerous varied reaction conditions formation of the mono-substituted ligand (DMIP) was favoured. The steric bulk of the

diisopropyl groups, and their relative proximity to one another on the triazine ring, is the likely reason for this.

Experimental

General

All reagents and solvents were purchased from Sigma-Aldrich Pty. Ltd. and used as received. Infrared spectra were measured on a Bruker Equinox 55 FT-IR fitted with a 71Judson MCT detector and Specac 'Golden Gate' diamond ATR. Electrospray ionization mass spectra (ESI-MS) were recorded with a Micromass (now Waters) ZMD with Waters alliance e2695 HPLC system for automatic sample injections. MeOH was the mobile phase and had a flow rate of 100 μL/min. Melting points were determined using a Bibby Stuart Scientific melting point apparatus SMP3. Microanalyses were performed by Campbell Microanalytical Laboratory, Department of Chemistry, University of Otago, Dunedin, New Zealand. Variable temperature magnetic susceptibility data were collected using either a Quantum Design MPMS 5 Superconducting Quantum Interference Device (SQUID) magnetometer or a MPMS XL-7 SQUID magnetometer, with a scan speed of 10 K/min followed by a one minute wait after each temperature change.

Differential scanning calorimetry (DSC) experiments were performed with a Thermal Analysis Instruments Q100 calorimeter. A typical 5–10 mg sample was sealed in a vented aluminium pan and placed in the furnace with a 50 mL/min dry nitrogen flow. The sample was analysed between –100 and + 25 °C at a scan rate of 5 K/min. The reference pan was an empty hermetic aluminium pan.

X-Ray crystallographic measurements on **1**, **2**, and **6** were performed at 100(2) K, with **7** collected at 173 K, at the Australian synchrotron MX1 beam-line operating at λ = 0.71073 Å. The data collection and integration for **1**, **2**, **6** and **7** were performed within Blu-Ice[22] and XDS[23] software programs. X-ray crystallographic measurements for **4** were collected on an Oxford Gemini Ultra diffractometer at 123(2) K with Cu-Kα radiation (λ = 1.5418 Å). Diffraction data analysis was performed using CrysAlisPro, Oxford Diffraction Ltd., Version 1.171.34.36. Empirical absorption correction was performed using spherical harmonics, implemented in SCALE3 ABSPACK scaling algorithm.[24]

X-ray crystallographic measurements on **3** and **5** were performed at 123(2) K using a Bruker Smart Apex X8 diffractometer with Mo-Kα radiation, λ = 0.71073 Å. Diffraction data analysis was performed using SAINT+ within the APEX2 software package and corrected for absorption using the Bruker SADABS program.[25]

Crystallographic data and refinement parameters for **1**-**7**, given in Table 6, were solved by direct methods (SHELXS-97), and refined (SHELXL-97) by full least-squares on all F^2 data.[26] All other non-hydrogen atoms in **1**-**7** are refined anisotropically and all hydrogen atoms are placed in calculated positions (unless otherwise specified). The crystal structure of **7** contains positional disorder in one of the alkyl arms of the DHDT ligand. The disorder is located on the hexyl group comprising carbon atoms C53 to C58. Atoms C56 and C57 were found to be disordered over two positions and the relative occupancies were refined but constrained to give full occupancy in total. In order to model hydrogen atoms correctly, C55 and C58 were duplicated (to give C55' and C58') and constrained to occupy the same xyz coordinates and have the same anisotropic displacement parameters. SADI restraints were placed on atom pairs C55/C56, C56/C57, C57/C58 and C55'/C56', C56'/C57', C57'/C58'.

Unsurprisingly, the structure showed signs of significant disorder in the alkyl chains of the ligands, particularly (but not exclusively) for the Co2 complex. As a result, many of the atoms were refined isotropically, particularly towards the ends of the chains. Furthermore, atoms C17 to C23 were refined with a common isotropic atomic displacement parameter using the EADP instruction in SHELX-97,[26] as were atoms C45 to C47. The isotropic atomic displacement parameters of C135 to C139 were fixed to 0.25. The two atoms in the alkyl chain after C166 were refined over two equally occupied positions (C167/C168, and C267/C268) and all four positions were refined with a common isotropic atomic displacement parameter. The five atoms in the alkyl chain after C171 were refined over two equally occupied positions (C172 to C176, and C272 to C276) and the isotropic atomic displacement parameters of C173 to C176 were fixed to 0.25. The atom in the alkyl chain after C183 was refined over two equally occupied positions (C184 and C284) and the isotropic atomic displacement parameters of both positions were fixed to 0.25. Hydrogen atoms were not assigned to a small number of atoms on the alkyl chains due to the disorder.

The large R_1 values for a number of the structures are due to a combination of disorder in the long alkyl chain moieties of the ligands, combined with small crystal sizes which required synchrotron radiation for structure determination.

CCDC numbers **1**, 1050210, **2**, 1050211, **3**, 1050212, **4** (110 K), 1050213, **4** (140 K), 1050214, **4** (185 K), 1050215, **5**, 1050216, **6**, 1050217, **7**, 1050218.

Photomagnetic characterisation for compounds **1**, **2** and **4** were carried out at CNRS, Université de Bordeaux, ICMCB, with a set of photodiodes coupled through an optical fibre into the cavity of the MPMS-55 Quantum design SQUID magnetometer operating at 2 T. Samples were prepared as a thin layer (ca. 0.1 mg) to promote full penetration of the irradiated light. The sample weight was obtained by comparing its thermal spin transition behaviour with an accurately weighed sample. The sample was first slowly cooled to 10 K by ensuring that potential trapping of HS species at low temperatures did not occur. Irradiation to photosaturation was carried out a number of times at different wavelengths to determine which source was most efficient at a power intensity of 5 mW cm^{-2} (to prevent warming of the sample). Samples were then cooled to 10 K and irradiated with green light (λ = 510 nm (for **1** and **2** and **4**)) until photosaturation was reached. Then, in the absence of irradiation, the temperature was increased at a rate of 0.3 K min^{-1}. The extreme of the $\delta\chi MT/\delta T$ *vs.* T plot gave the T(LIESST) values for compounds **1**, **2** and **4**, defined as the temperature for which the light-induced HS information is erased. At 10 K, compounds **1**, **2** and **4** were again irradiated to photosaturation, and in the absence of irradiation the relaxation kinetics were measured at the desired temperature.

Synthesis of Ligands and Precursors

4,6-dichloro-*N,N*-di-2-pyridinyl-1,3,5-triazin-2-amine was made following the synthetic procedure given by Ross, *et al*.[10]

DMIP - 6-chloro-N^2,N^2-diisopropyl-N^4,N^4-di(pyridine-2-yl)-1,3,5-triazine-2,4-diamine

4,6-dichloro-N,N-di-2-pyridinyl-1,3,5-triazin-2-amine (1.2 g, 3.77 mmol), diisopropylamine (0.82 g, 8.14 mmol) and diisopropylethylamine (~2 ml) were dissolved in 20 ml

MeCN:toluene (1:1 (v/v)) and refluxed for 12 hours. After this time the solution was filtered and a white crystalline solid of excess diisopropylamine was separated from the solution. The filtrate was then reduced *in vacuo* to give a brown oily product which was then washed with 50 ml H_2O and extracted with $CHCl_3$ (2 × 40 ml). The combined organic extracts were then reduced *in vacuo* and the product purified via column chromatography (SiO_2, 1:1 Et_2O:Hexane (v/v), R_f = 0, THF R_f = 0.83). Mw 383.88; Yield 0.95 g (65 %); ^{1}H-NMR (400 MHz, $CDCl_3$) δ 8.369 (2H, ddd, J = 4.8, 1.8, 0.8 Hz), 7.692 (2H, ddd, J = 11.4, 9.6, 9.6 Hz), 7.490 (2H, dm, J = 3.6 Hz), 7.079 (2H, ddd, J = 7.4, 4.8, 1.2 Hz), 4.738 (1H, s), 3.614 (1H, s), 1.117 (6H, d, J = 6.4 Hz), 0.995 (6H, d, J = 6.8 Hz); ^{13}C-NMR (600 MHz, $CDCl_3$) 168.961, 165.384, 163.599, 155.107, 148.899, 137.674, 122.946, 121.379, 67.967, 46.629, 45.788, 25.615; IR (cm^{-1}) 3053 (s), 2975 (s), 1564 (s), 1487 (s), 1456 (s), 1408 (s), 1381 (s), 1362 (s), 1315 (s), 1298 (m), 1285 (s), 1251 (m), 1218 (s), 1172 (s), 1145 (m), 1104 (m), 1076 (m), 1051 (s), 1024 (s), 1006 (s), 994 (s), 894 (s), 814 (s), 798 (s), 780 (s), 742 (m), 681 (s), 668 (m), 623 (m); MS (ESI+) *m/z*: 384.0 $[M+H]^+$; Anal. Found C 59.67, H 6.00, N 25.24; Calcd. for $C_{19}H_{22}Cl_1N_7$, C 59.45, H 5.78, N 25.54.

DPDT - *N*^{2},*N*^{2},*N*^{4},*N*^{4}-tetra-n-propyl-*N*^{6},*N*^{6}-di(pyridin-2-yl)-1,2,5-triazine-2,4,6-triamine

4,6-dichloro-*N,N*-di-2-pyridinyl-1,3,5-triazin-2-amine (1.3 g, 4.0 mmol), dipropylamine (0.90 g, 8.9 mmol), diisopropylethylamine (3 ml) were dissolved in 40 ml MeCN:toluene (1:1) (v:v) and refluxed overnight. After this time the solution was then reduced *in vacuo* and the remaining oily product washed with H_2O (2 × 30 ml) and the product extracted with $CHCl_3$ (2 × 40 ml). The combined organic extracts were reduced *in vacuo* to give a red-orange oil. This was purified via column chromatography (SiO_2, 1:1 Et_2O:Hexane (v/v), R_f = 0, DCM R_f = 0.71); Mw 448.61; Yield 0.79 g (44 %); ^{1}H-NMR (400 MHz, DMSO-*d6*) δ 8.271 (2H, ddd, J = 4.8, 2.0 , 0.8 Hz), 7.771 (2H, ddd, J = 8.0, 6.6, 2.0), 7.592 (2H, dm, J = 8.4 Hz), 7.151 (2H, ddd, 7.4, 4.8, 1.2), 3.375 (4H, t, J = 7.2 Hz), 3.116 (4H, t, J = 8.0 Hz), 1.537 (4H, m), 1.378 (4H, m), 0.845 (6H, t, J = 7.6 Hz), 0.644 (6H, t, J = 7.6 Hz); ^{13}C-NMR (400 MHz, DMSO-*d6*) δ 165.212, 164.095, 155.902, 147.756, 136.616, 122.546, 120.100, 48.510, 20.877, 11.264; IR (cm^{-1}) 2957 (s), 2930 (s), 2870 (s), 1588 (s), 1543 (s), 1525 (s), 1492 (s), 1461 (s), 1422 (s), 1393 (s), 1369 (s), 1330 (s), 1314 (s), 1296 (s), 1254 (m), 1233 (m), 1182 (s), 1143 (w), 1091 (w), 996 (w), 893 (s), 849 (m), 806 (s), 771 (s), 735 (m), 628 (s), 639 (s), 617 (s); MS (ESI+) *m/z*: 449.2 $[M+H]^+$; 471.2 $[M+Na]^+$; Anal. Found C 66.94, H 8.03, N 24.91; Calcd. for $C_{25}H_{36}N_8$, C 66.93, H 8.09, N 24.98.

DHDT - *N*^{2},*N*^{2},*N*^{4},*N*^{4}-tetra-n-hexyl-*N*^{6},*N*^{6}-di(pyridin-2-yl)-1,2,5-triazine-2,4,6-triamine

The synthesis of DHDT follows a similar synthetic route to that previously published by Ross *et al*.,[10] for which the n-butyl analogue was described. The current method, however, uses the addition of hexane for the extraction of unreacted amine.

4,6-dichloro-N,N-di-2-pyridinyl-1,3,5-triazin-2-amine, (2.7 g, 8.5 mmol), dihexylamine (3.9 g, 21.2 mmol) and diisopropylethylamine (3.6 ml, 21.2 mmol) were dissolved in 20 ml MeCN:toluene (1:1 v:v) and the solution refluxed under nitrogen overnight. After this time the solvent was removed *in vacuo* and the resultant brown oil washed with 50 ml deionised H_2O and extracted with $CHCl_3$ (2 × 50 ml). The combined organic extracts were reduced *in vacuo* to give another brown oil. To this, 20 ml hexane was added and the solution refluxed for 20 mins. The product was then filtered and the orange filtrate was reduced *in vacuo*. The product was then purified via column chromatography (SiO_2, 1:1 Et_2O:Hexane (v/v), R_f = 0.88). Mw 616.93; Yield 0.96 g (18 %); MP 49.2 – 50.6° C; ^{1}H-NMR (400 MHz, DMSO-*d6*) δ 8.313 (2H, ddd, J = 7.2, 4.8, 2.0), 7.790 (2H, ddd, J = 6.0 4.8, 1.6 Hz), 7.620 (2H, dm, J = 8.0 Hz), 7.191 (2H, ddd, J = 5.2 Hz, 4.8 Hz, 0.8 Hz), 3.451 (4H, t, J = 7.2 Hz), 3.196 (4H, t, J = 8.0 Hz), 1.168 (32H, m), 0.893 (12H, m); ^{13}C-NMR (400 MHz, $CDCl_3$) δ 165.24, 164.02, 155.93, 147.73, 136.57, 122.49, 120.08, 46.66, 31.19, 27.62, 26.12, 22.11, 13.81; IR (cm^{-1}) 2955 (sh), 2922 (s), 2852 (s), 1598 (s), 1547 (s), 1526 (s), 1499 (m), 1463 (s), 1424 (s), 1397 (s), 1375 (m), 1328 (m), 1297 (m), 1258 (s), 1232 (s), 1214 (w), 1148 (s), 1099 (s), 1050 (m), 1025 (m), 996 (s), 867 (s), 806 (s), 772 (s), 736 (s), 697 (s), 683 (m), 641 (s), 619 (s); MS (ESI+) *m/z*: 617.0 $[M+H]^+$; Anal. Found C 72.28, H 9.90, N 18.34; Calcd. for $C_{37}H_{60}N_8$, C 72.03, H 9.80, N 18.16.

DODT - *N*^{2},*N*^{2},*N*^{4},*N*^{4}-tetra-n-octyl-*N*^{6},*N*^{6}-di(pyridin-2-yl)-1,2,5-triazine-2,4,6-triamine

4,6-dichloro-N,N-di-2-pyridinyl-1,3,5-triazin-2-amine, (1.8 g, 5.66 mmol), dioctylamine (3 g, 12.4 mmol) and diisopropylethylamine (3.6 ml, 21.2 mmol) were dissolved in 20 ml MeCN:toluene (1:1 v:v) and the solution refluxed under nitrogen overnight. After this time the solvent was removed *in vacuo* and the resultant brown oil washed with 50 ml deionised H_2O and extracted with $CHCl_3$ (2 × 50 ml). The combined organic extracts were reduced *in vacuo* to give a brown oil. To this, 20 ml hexane was added and the solution refluxed for 20 mins. The product was then filtered and the orange filtrate was reduced *in vacuo*. The product was then purified via column chromatography (SiO_2, 1:1 Et_2O:Hexane (v/v), R_f = 0.84); Mw 729.14; Yield 1.38 g (33 %); MP 60.3 – 61.1°C; ^{1}H-NMR (400 MHz, $CDCl_3$) 8.366 (2H, ddd, J = 4.8, 1.2, 0.8 Hz), 7.662 (4H, m), 7.035 (2H, ddd, 6.0, 4.0, 2.4), 3.409 (4H, t, J = 7.6 Hz), 3.176 (4H, t, J = 7.6 Hz), 1.270 (48H, m), 0.878 (12H, m); ^{13}C-NMR (400 MHz, $CDCl_3$) δ 165.73, 1654.64, 156.57, 148.27, 136.43, 123.13, 119.86, 47.35, 31.86, 29.55, 29.41, 28.23, 27.15, 22.71, 14.10; IR (cm^{-1}) 2953 (sh), 2918 (s), 2850 (s), 1589 (s), 1548 (s), 1526 (s), 1500 (s), 1464 (m), 1424 (s), 1395 (s), 1374 (s), 1328 (m), 1296 (m), 1261 (m), 1233 (m), 1147 (m), 1103 (m), 1051 (m), 997 (w). 938 (m), 859 (s), 806 (s), 772 (s), 748 (s), 736 (s), 720 (s), 698 (s), 682 (s), 642 (s), 619 (s); MS (ESI+) *m/z*: 729.6 $[M+H]^+$; Anal. Found C 74.12, H 10.35, N 15.49; Calcd. for $C_{45}H_{76}N_8$, C 74.13, H 10.51, N 15.37.

Metal Complex Syntheses

$[Fe^{II}(DMIP)_2(NCS)_2]$ (1)

DMIP (15 mg, 0.039 mmol), NaNCS (3.2 mg, 0.039 mmol), $Fe(ClO_4)_2 \cdot xH_2O$ (4.9 mg, 0.019 mmol) and ~10 mg ascorbic acid were dissolved in 4 ml MeOH and the solution stirred for 30 minutes. After this time, the product was filtered and the filtrate diffused with diethyl ether. Very small yellow crystals of X-ray diffraction quality formed after one week. Mw 939.77; Yield 3 mg (16 %); IR (cm^{-1}, room temperature) 2964 (m), 2058 (s), 1579 (s), 1561 (s), 1493 (s), 1477 (s), 1466 (s), 1407 (s), 1382 (s), 1363 (s), 1308 (s), 1290 (m), 1238 (m), 1177 (s), 1151 (w), 1113 (w), 1018 (m), 999 (m), 820 (w), 796 (m), 785 (m), 755 (m), 674 (m); Anal. Found C 50.02, H 4.92, N 22.44; Calcd. for $C_{40}H_{44}Fe_1N_{16}Cl_2S_2$ + 2MeOH C 50.25, H 5.22, N 22.32. Calcd. for $C_{40}H_{44}Fe_1N_{16}Cl_2S_2$, C 51.11, H 4.71, N 23.85.

$[Fe^{II}(DMIP)_2(NCSe)_2]$ (2)
DMIP (15 mg, 0.039 mmol), KNCSe (5.6 mg, 0.039 mmol), $Fe(ClO_4)_2 \cdot xH_2O$ (4.9 mg, 0.019 mmol) and ~10 mg ascorbic acid were dissolved in 4 ml MeOH and the solution stirred for 30 mins. After this time, the product was filtered and the filtrate diffused with diethyl ether. Very small yellow crystals of X-ray diffraction quality formed after one week. Mw 1033.56; Yield 9.2 mg (46 %); IR (cm^{-1}, room temperature) 2963 (w), 2062 (s), 1579 (sh), 1561 (s), 1493 (s), 1465 (s), 1407 (s), 1381 (s), 1361 (s), 1308 (s), 1290 (m), 1238 (m), 1150 (s), 999 (m), 819 (m), 786 (m), 673 (m); Anal. Found C 44.63, H 4.30, N 20.47; Calcd. for $C_{40}H_{44}Fe_1N_{16}Cl_2Se_2$ + 4MeOH C 45.49, H 5.21, N 20.47. Calcd. for $C_{40}H_{44}Fe_1N_{16}Cl_2Se_2$, C 46.48, H 4.28, N 21.68.

$[Fe^{II}(DPDT)_2(NCS)_2]$ (3)
DPDT (10 mg, 0.022 mmol), NaNCS (1.8 mg, 0.02 mmol) and $Fe(ClO_4)_2 \cdot xH_2O$ (2.8 mg, 0.01 mmol) were dissolved in a 4 ml MeOH and stirred for 30 mins. After this time the solution was left to sit and slowly evaporate. After 72 hours, small yellow block crystals had formed and were of X-ray diffraction quality. Mw 1068.50; Yield 3 mg (25 %); IR (cm^{-1}, room temperature) 2961 (s), 2928 (s), 2870 (s), 2054 (s), 1600 (s), 1572 (s), 1556 (s), 1503 (s), 1476 (s), 1463 (s), 1425 (s), 1364 (s), 1342 (s), 1303 (m), 1236 (s), 1153 (w), 1083 (w), 1015 (m), 823 (w), 805 (m), 771 (m), 753 (m), 680 (m), 627 (m); Anal. Found C 58.53, H 6.92, N 23.78; Calcd. for $C_{52}H_{72}Fe_1N_{18}S_2$, C 58.41, H 6.79, N 22.58.

$[Fe^{II}(DPDT)_2(NCSe)_2]$ (4)
DPDT (20 mg, 0.046 mmol), KNCSe (6.3 mg, 0.043 mmol) and $Fe(ClO_4)_2 \cdot xH_2O$ (5.6 mg, 0.022 mmol) were dissolved in 4 ml MeOH, with light heating and stirred for one hour. After this time the solution was left to sit for an hour and then filtered. The filtrate was left to slowly evaporate. After one week, small yellow block crystals had formed and were of X-ray diffraction quality. Mw 1163.01; Yield 8 mg (31 %), IR (cm^{-1}, room temperature) 2959 (s), 2926 (s), 2870 (s), 2060 (s), 1601 (s), 1572, 1503 (s), 1475 (s), 1463 (s), 1425 (s), 1364 (s), 1342 (s), 1303 (s), 1236 (s), 1178 (w), 1152 (w), 1096 (m), 1082 (m), 1015 (w), 984 (w), 861 (w), 824 (m), 805 (m), 771 (m), 754 (m), 680 (m), 628 (m); Anal. Found C 53.47, H 6.13, N 21.44; Calcd. for $C_{52}H_{72}Fe_1N_{18}Se_2$, C 52.70, H 6.24, N 21.68.

Journal Name RSCPublishing

ARTICLE

Table 6. **Crystallographic data for complexes 1-7**.

Compound	1	2	3	4 (110K)	4(140K)	4(185K)
Formula	$C_{40}H_{44}Cl_2Fe_1N_{16}S_2$	$C_{40}H_{44}Cl_2Fe_1N_{16}Se_2$	$C_{52}H_{72}Fe_1N_{18}S_2$	$C_{52}H_{72}Fe_1N_{18}Se_2$	$C_{52}H_{72}Fe_1N_{18}Se_2$	$C_{52}H_{72}Fe_1N_{18}Se_2$
Mw (g mol^{-1})	939.77	1033.56	1068.5	1163.05	1163.05	1163.05
T (K)	100	100	123	110	110	110
Crystal system	Monoclinic	Monoclinic	Orthorhombic	Orthorhombic	Orthorhombic	Orthorhombic
Space group	$P2_1/n$	$P2_1/n$	*Pbcn*	*Pbcn*	*Pbcn*	*Pbcn*
Z	2	2	4	4	4	4
a (Å)	11.530(2)	11.443(2)	21.5412(9)	21.5709(15)	21.4283(11)	21.4596(12)
b (Å)	15.840(3)	15.924(3)	14.7267(6)	14.7251(7)	14.7993(7)	14.8312(7)
c (Å)	12.190(2)	12.050(2)	17.5670(7)	17.349(2)	17.6804(13)	17.8149(14)
β (°)	103.79(3)	103.92(3)	90	90	90	90
V (Å^3)	2162.1(7)	2131.2(7)	5572.8(4)	5510.6(8)	5606.9(6)	5670.0(6)
ρ_{calc} (g cm^{-3})	1.02	1.611	1.274	1.402	1.378	1.362
μ (mm^{-1})	0.493	2.24	0.398	1.6848	1.62	1.602
Measured/independent (R_{int}) Reflections	35608/5373(0.0763)	15605/4114(0.1074)	153684/7925(0.0451)	36061/ 9144(0.0832)	37336/9275((0.0655)	37776/9379(0.0697)
Observed reflections [I > 2σ(I)]	4625	2854	6158	4838	5211	4756
R_1[a], wR_2[b] [I > 2σ(I)]	0.0826, 0.2069	0.0638, 0.1586	0.0357, 0.0785	0.0700, 0.1714	0.0534, 0.1095	0.0506, 0.1105
R_1, wR_2 (all data)	0.0929, 0.2142	0.0956, 0.1758	0.0534, 0.0863	0.1396, 0.2254	0.1209, 0.1440	0.1313, 0.1491
Goodness-of-fit on F^2	1.089	1.044	1.002	1.058	1.023	1.024

Compound	5	6	7
Formula	$C_{76}H_{120}Fe_1N_{18}S_2$	$C_{76}H_{120}Co_1N_{18}S_2$	$C_{92}H_{152}Co_1N_{18}S_2$
Mw (g mol^{-1})	1405.87	1408.95	1633.38
T (K)	123	100	173
Crystal system	Monoclinic	Orthorhombic	Triclinic
Space group	*C*2/*c*	$P2_12_12_1$	*P*-1
Z	8	4	4
a (Å)	33.105(7)	8.9280(18)	15.933(3)
b (Å)	27.231(5)	27.219(5)	24.420(5)
c (Å)	18.266(4)	32.757(7)	28.254(3)
β (°)	90	90	101.58(3)
V (Å^3)	15884(6)	7960(3)	9716(3)
ρ_{calc} (g cm^{-3})	1.176	1.176	1.117
μ (mm^{-1})	0.295	0.32	0.271
Measured/independent (R_{int}) Reflections	57940/16024(0.0622)	140433/20551(0.1194)	89372/25639(0.1163)
Observed reflections [I > 2σ(I)]	16024	16058	14771
R_1[a], wR_2[b] [I > 2σ(I)]	0.1201, 0.3258	0.0513, 0.1220	0.1314, 0.3565
R_1, wR_2 (all data)	0.1272, 0.3291	0.0743, 0.1365	0.1828, 0.3986
Goodness-of-fit on F^2	1.121	1.045	1.376

[a] $R_1 = \sum||F_o| - |F_c||/\sum|F_o|$. [b] $wR_2 = \{\sum[w(F_o^2\sum F_c^2)^2]/\sum[w(F_o^2)]\}^{1/2}$

Journal Name RSCPublishing

ARTICLE

$[Fe^{II}(DHDT)_2(NCS)_2]$ (5)
DHDT (20 mg, 0.032 mmol), NaNCS (5.3 mg, 0.064 mmol), $Fe(ClO_4)_2 \cdot xH_2O$ (8.1 mg, 0.032 mmol) and ~10 mg ascorbic acid were dissolved in 5 ml MeOH and stirred for 30 mins. After this time, the solution was filtered and the filtrate left to slowly evaporate. The product crystallised as small yellow block shaped crystals. Mw 1405.86; Yield <1 mg (~10 %); IR (cm^{-1}, room temperature) 2924 (s), 2854 (s), 2051 (s), 1555 (sh), 1505 (s), 1476 (s), 1463 (s), 1427 (s), 1360 (s), 1303 (s), 1225 (m), 1106 (w), 805 (w), 774 (w), 752 (w); Anal. Found C 64.95, H 8.86, N 17.97; Calcd. for $C_{76}H_{120}Fe_1N_{18}S_2$, C 64.93, H 8.60, N 17.93.

$[Co^{II}(DHDT)_2(NCS)_2]$ (6)
DHDT (20 mg, 0.03 mmol), NaNCS (2.6 mg, 0.03 mmol) and $Co(BF_4)_2 \cdot xH_2O$ (5.5 mg, 0.01 mmol) were dissolved in 5 ml MeOH and stirred for 30 mins. The solution was left to slowly evaporate. After 72 hours, small yellow block-shaped crystals had formed. Mw 1408.95; Yield 22 mg (71 %); IR (cm^{-1}, room temperature) 2924 (s), 2854 (s), 2059 (s), 1601 (s), 1556 (s), 1515 (s), 1477 (s), 1465 (s), 1425 (s), 1364 (s), 1308 (s), 1234 (m), 1106 (w), 1017 (w), 806 (m), 775 (m), 752 (m), 680 (m), 630 (m); Anal. Found C 64.94, H 8.73, N 17.89; Calcd. for $C_{76}H_{120}Co_1N_{18}S_2$, C 64.79, H 8.58, N 17.89.

$[Co^{II}(DODT)_2(NCS)_2]$ (7)
DODT (20 mg, 0.027 mmol), NaNCS (2.2 mg, 0.027 mmol) and $Co(ClO_4)_2 \cdot xH_2O$ (5.0 mg, 0.013 mmol) were dissolved in 5 ml MeOH and stirred for 30 minutes. The solution was left to slowly evaporate. After 72 hours, small yellow block-shaped crystals had formed. Mw 1633.38; Yield 16 mg (71 %); IR (cm^{-1}, room temperature) 2921 (s), 2851 (s), 2062 (s), 1601 (s), 1571 (s), 1556 (s), 1502 (s), 1477 (s), 1464 (s), 1425 (s), 1390 (s), 1363 (s), 1309 (s), 1237 (s), 1152 (m), 1110 (m), 1052 (m), 1017 (m), 806 (s), 775 (s), 752 (s), 680 (m), 629 (m); Anal. Found C 67.59, H 9.55, N 15.61; Calcd. for $C_{92}H_{156}Co_1N_{18}S_2$, C 67.65, H 9.38, N 15.44.

Conclusions

Four new dipyridylamino-substituted *s*-triazine ligands, each with different alkyl chain length moieties, designed to influence packing arrangements and intermolecular interactions, have been incorporated into mononuclear Fe^{II} or Co^{II} complexes. The magnetostructural characterisation of four new Fe^{II} SCO compounds has been presented, as well as that of three new HS Fe^{II} and Co^{II} compounds. Compounds **1**, **2** and **4** were found to give well resolved photomagnetic/LIESST behaviour and relaxation kinetics. Investigations into order-disorder structural rearrangements have been performed, particularly for complex **4** which was found to exhibit an abrupt SCO, although no such behaviour was observed for **4** or for any of the other complexes reported here.

Finally, the crystallographic order observed in complexes **1** to **7** show that mesophases or liquid crystals are not formed under the conditions used. Presumably, longer alkyl chains than C_8 will be required, as well as use of high temperatures to explore any mesophases by techniques such as optical microscopy, DSC, powder X-ray diffraction.[7]

Acknowledgements

K.S.M. thanks the Australian Research Council for a Discovery grant, Dr I. A. Gass for help with DSC studies and Dr W. Phonsri for help with journal templates. J.-F. L. and G. C. would like to thank the Aquitaine Region for supporting the development of the ICPA (International Center of Photomagnetism in Aquitaine) at the ICMCB. Portions of this work were carried out on the MX1 Macromolecular Crystallography beamline at the Australian Synchrotron, Victoria, Australia.

Notes and references

[a] School of Chemistry, Building 23, 17 Rainforest Walk, Monash University, Clayton, Victoria, 3800, Australia. Fax: +61-3-9905-4597; Tel: +61-3-9905-4512; E-mail: keith.murray@monash.edu
[b] CNRS, Université de Bordeaux, ICMCB, 87 avenue du Dr. A.Schweitzer, 33608, Pessac, France.
[c] Department of Chemistry, Faculty of Science, King Abdulaziz University, Jeddah, Saudi Arabia.
† Electronic Supplementary Information (ESI) available: [Crystallographic packing diagrams, Figs S1 – S4; LIESST data, Figs S5 – S8]. See DOI: 10.1039/b000000x/

1. (a) M. A. Halcrow, Ed. *Spin Crossover Materials. Properties and Applications*, Wiley, London, 2013; (b) Special Issue: Spin-Crossover Complexes (Cluster Issue), *Eur. J. Inorg. Chem*., 2013, 5-6.
2. J. L. Serrano, *Metallomesogens: Synthesis, Properties, and Applications*, John Wiley & Sons, New York, 2008.
3. (a) M. Seredyuk, A. B. Gaspar, V. Ksenofontov, Y. Galyametdinov, J. Kusz and P. Gütlich, *J. Am. Chem. Soc.*, 2008, **130**, 1431; (b) K. Kuroiwa, H. Kikuchib and N. Kimizuka, *Chem. Commun.*, 2010, **46**, 1229; (c) S. Hayami, R. Moriyama, A. Shuto, Y. Maeda, K. Ohta and K. Inoue, *Inorg. Chem*., 2007, **46**, 1789.
4. Y. Galyametdinov, V. Ksenofontov, A. Prosvirin, I. Ovchinnikov, G. Ivanova, P. Gütlich and W. Haase, *Angew. Chem. Int.,* 2001, **40**, 4269.
5. (a) A. B. Gaspar, M. Seredyuk and P. Gütlich, *Coord. Chem. Rev*., 2009, **253**, 2399; (b) A. B. Gaspar and M. Seredyuk, *Coord. Chem. Rev.* 2014, **268**, 41.
6. (a) Chapter 12: M. A. Halcrow, *Spin Crossover Materials. Properties and Applications*, ed., Wiley, London, 2013; (b) S. Hayami, M. R. Karim and Y. H. Lee, *Eur. J. Inorg. Chem*., 2013, 683.
7. (a) P. Grondin, D. Siretanu, O. Roubeau, M-F. Achard and R.Clérac, *Inorg. Chem.* 2012, **51**, 5147; (b) O. Roubeau, B. Agricole, R. Clérac and S. Ravaine, *J. Phys. Chem. B*, 2004, **108**, 15110.

8. See for example: (a) S. Hayami, Y. Shigeyoshi, M. Akita, K. Inoue, K. Kato, K. Osaka, M. Takata, R. Kawajiri, T. Mitani and Y. Maeda, *Angew. Chem., Int. Ed.*, 2005, **44**, 4899; (b) S. Hayami, D. Urakami, Y. Kojima, H. Yoshizaki, Y. Yamanoto, K. Kato, A. Fuyuhiro, S. Kawata and K. Inoue, *Inorg. Chem.*, 2010, **49**, 1428; (c) A. Kaiba, H. J. Shepherd, D. Fedaoui, P. Rosa, A. E. Goeta, N. Rebbani, J.-F. Létard and P. Guionneau, *Dalton Trans.*, 2010, **39**, 2910; (d) Chapter Five: M. A. Halcrow, *Spin Crossover Materials. Properties and Applications*, ed., Wiley, London, 2013.
9. M. Seredyuk, M. C. Muñoz, M. Castro, T. Romero-Morcillo, A. B. Gaspar and J. A. Real, *Chem. Eur. J.*, 2013, **19**, 6591.
10. T. M. Ross, B. Moubaraki, K. S. Wallwork, S. R. Batten and K. S. Murray, *Dalton Trans.*, 2011, **40**, 10147.
11. P. Guionneau, M. Marchivie, G. Bravic, J.-F. Létard and D. Chasseau, *Top. Curr. Chem.*, 2004, **234**, 97.
12. M. Marchivie, P. Guionneau, J.-F. Létard and D. Chasseau, *Acta Crystallogr., Sect. B.*, 2005, **61**, 25.
13. V.A. Money, C. Carbonera, M.A. Halcrow, J.A.K. Howard, J.-F. Létard, *Chem. Eur. J.*, 2007, **13**, 5503.
14. (a) M. Sorai and S. Seki, *J. Phys. Chem. Solids*, 1974, **35**, 555; (b) M. Sorai, *Top. Curr. Chem.*, 2004, **235**, 153.
15. (a) B. N. Figgis and M. A. Hitchman, *Ligand Field Theory and its Applications*, Wiley-VCH, New York, 1966; (b) F. E. Mabbs, D. J. Machin, *Magnetism and Transition Metal Complexes*, Dover Publishers, New York, 2008; (c) O. Kahn, *Molecular Magnetism*, Wiley-VCH, New York, 1993.
16. (a) N. Paradis, G. Chastanet and J.-F. Létard, *Eur. J. Inorg .Chem.* 2012, 3618 ; (b) N. Paradis, G. Chastanet, F. Varret and J.-F. Létard, *Eur. J. Inorg. Chem.* 2013, 698 ; (c) F. Varret, K. Boukheddaden, G. Chastanet, N. Paradis and J.-F. Létard, *Eur. J. Inorg. Chem*, 2013, 763.
17. A. Hauser, J.P. Alder and P. Gütlich, *Chem. Phys. Lett.* 1988, **152**, 468.
18. A. Hauser, *Coord. Chem. Rev.* 1991, **111**, 275.
19. G. Dupouy, M. Marchivie, S. Triki, J. Sala-Pala, C.J. Gómez-García, S. Pillet, C. Lecomte, J.-F. Létard, *Chem. Comm*. 2009, 3404.
20. (a) S. Hayami, Y. Shigeyoshi, M. Akita, K. Inoue, K. Kato, K. Osaka, M. Takata, R. Kawajiri, T. Mitani and Y. Maeda, *Angew. Chem. Int. Ed.,* 2005, **117**, 4977.
21. J.-F. Létard, *J. Mater. Chem*., 2006, **16**, 2550.
22. T. M. McPhillips, S. E. McPhillips, H. J. Chiu, A. E. Cohen, A. M. Deacon, P. J. Ellis, E. Garman, A. Gonzalez, N. K. Sauter, R. P. Phizackerley, S. M. Soltis and P. Kuhn, Blu-Ice and the Distributed Control System: software for data acquisition and instrument control at macromolecular crystallography beamlines, *J. Synchrotron Radiat.*, 2002, **9**, 401.
23. W. Kabsch, *J. Appl. Crystallogr*., 1993, **26**, 795.
24. CrysAlisPro, Oxford Diffraction Ltd., Version 1.171.35.15 (release 03-08-2011 CrysAlis171 .NET).
25. G. M. Sheldrick, SADABS, Program for area detector adsorption correction, Institute for Inorganic Chemistry, University of Göttingen, Germany, 1996.
26. (a) G. M. Sheldrick, SHELXL-97, Program for refinement of crystal structures, University of Göttingen, Germany, 1997; (b) A. L. Spek, *Acta Crystallogr., Sect. A: Fundam. Crystallogr*., 1990, **46**, C34.

2,2'-dipyridylamino-based ligands with substituted alkyl chain groups and their 0D-M(II) spin crossover complexes

TOC

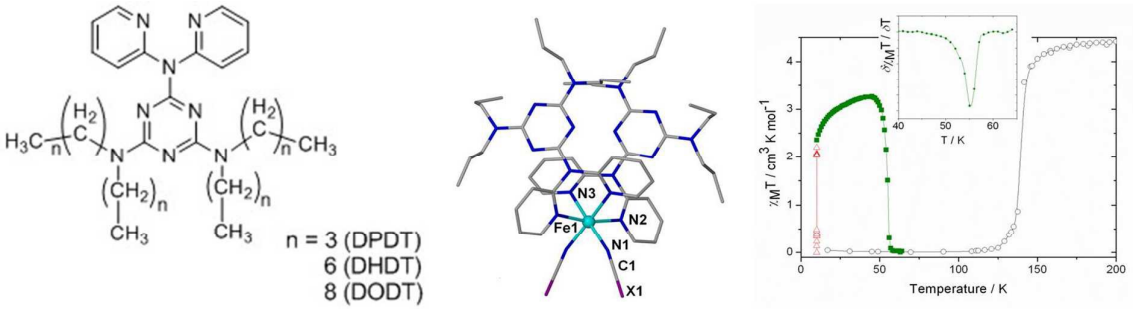

A family of iron(II) and cobalt(II) complexes of alkyl-chain appended triazine- 2,2'-dipyridylamino-based N, N-donor ligands has been explored for their spin crossover d^6 (Fe^{II}) and d^7(Co^{II}) properties. Fundamental structural, magnetic and photomagnetic (Light induced excited spin state trapping) features are described. All complexes are crystalline, with ordered structures, and no soft matter features are evident under the conditions explored.